Fatigue Crack Initiation on Plasma Ion Nitrided Steel with and Without Hydrogen

M. A. Zampronio[1], P. E. V. de Miranda[2], O. Bartier[3], D. Chicot[3], J. Lesage[3],
[1] *DFI/UEM, Av. Colombo 5790, CEP 87020-900 Maringá-PR, Brazil – mazampro@dfi.uem.br*
[2] *Laboratório de Hidrogênio, PEMM, COPPE/UFRJ, CP 68505, CEP 21945-970, Rio de Janeiro, Brazil – pmiranda@labh2.coppe.ufrj.br*
[3] *GRCMA, IUT GMP, Rennes, France – Olivier.Bartier@univ-Rennes1.fr*
[4,5] *LML, UST Lille, P. O. Box 179, 59653 Villeneuve d'Ascq, France – Didier.Chicot@univ-lille1.fr; Jacky.Lesage@univ-lille1.fr*

Abstract

Fatigue crack initiation was studied on a type API 5L X-65 steel in the conditions as received and plasma ion nitrided, using optical microscopy with Nomarski interferometry. The nitriding process gave origin to a 550 µm thick surface modified layer, which contains a 5.1 µm thick white layer composed of nitrides and a diffusion zone. The as received steel presented surface deformation bands since the beginning of the fatigue test. Upon hydrogen charging, various surface micro-cracks were noted to nucleate and then give rise to the main fatigue crack. Fatigue crack initiation on the nitrided steel occurred sub-superficially. The fatigue tests performed upon hydrogen charging did not induce any surface modifications as compared to the as received steel. The fatigue limits due to hydrogen decreased from 350 to 300 MPa for the as received steel and from 660 to 500 MPa for the plasma ion nitrided steel.

Keywords: plasma ion nitriding; hydrogen embrittlement; fatigue crack initiation.

Introduction

Fatigue damage is one of the main causes of rupture of mechanical components, being originated by the simultaneous action of cyclic stress, tensile stress and plastic deformation. There is a limit under which the cyclic stress does not yield fracture. This work adopts the concept of fatigue limit as being the value of the cyclic stress underneath which no failure is observed after 10^7 cycles at a frequency of 30 Hz. Furthermore, it has been recently shown (1, 8) that no fatigue limit is observed by fatigue testing up to 10^{10} cycles with ultrasonic frequencies (20 kHz), although good agreement is found (8) with low frequency fatigue tests in the range of 10^5 to 10^7 cycles. The fatigue limit depends on the features of the material and of the environment. For example, it may be drastically reduced if the material is likely to absorb hydrogen (5). A solution for this problem would be to impede or to delay the introduction of hydrogen into the material by creating a metallurgical protective coating. This could consist of layers obtained by electrochemical deposition (3), by ion implantation (9, 10) or by pulsed (2) and continuous (4) plasma ion nitriding. The latter presents the advantage of introducing compressive residual stresses that associated with a very high surface hardness enhances fatigue resistance (7).

The objective of the present paper is to characterize, by means of optical metallography using Nomarski interferometry, the fatigue crack initiation and the surface fatigue damage of as received and plasma ion nitrided steel with and without previous hydrogen charging.

Materials and Methods

The material used in the present study was an API 5L X-65 type steel sheet with the following chemical composition (in wt%): C=0.11; Mn=1.05; S=0.005; P=0.014; Si=0.29; Al=0.035; Nb=0.02; V=0.0055; Ti=0.01; Ni=0.15; Cu=0.31; Ca=0.0074; Fe=balance. The microstructure consisted of banded pearlite in a matrix of ferrite. All samples, cut parallel to the rolling plane with a thickness of 2 mm, were metallographically polished. The continuous plasma ion nitriding was performed using the following conditions: temperature = 773 K, gas composition = 25 %N_2 + 75 %H_2, pressure = 5 mbar, nitriding time = 16h. Vickers micro-hardness profiling was performed using a load of 100 g after successive thickness reductions by electropolishing. Residual stresses

were determined by x-ray analysis of the γ' - Fe_4N (222) peak in the white layer and of the ferrite (220) peak in the diffusion zone. All samples were electrolytically hydrogen charged using NaOH 0.1 N as electrolyte at 50° C for the following currents and times: 180 mA, 4 h and 200 mA, 48 h, for the as received and nitrided steels, respectively.

Purely alternated flexion tests were performed at a frequency of 30 Hz. Fatigue limit at 10^7 cycles was obtained by the K not fractured samples method (K=2). The principle of this method is to apply decreasing cyclic loading stresses from a given level until two samples do not fracture after 10^7 cycles. A stress level 20% above the fatigue limit was chosen to perform tests in a few samples which were periodically interrupted in order to examine the surface micro morphology of the sample by optical microscopy using Nomarski interferometry.

Results

Figure 1 presents a scanning electron micrograph of the resulting microstructure after the plasma ion nitriding treatment. The nitriding process gave origin to a 550 μm thick surface modified layer, which contains a 5.1 μm thick white layer composed of nitrides and a diffusion zone that extends itself up to about 550 μm.

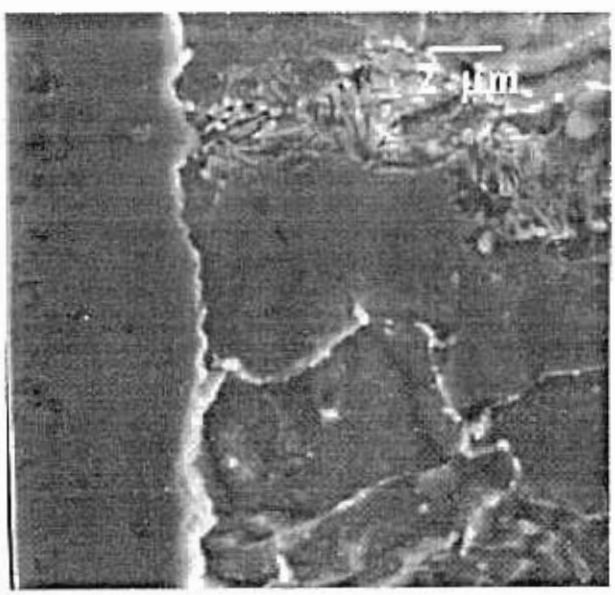

Fig. 1: Scanning electron micrograph of a sample that has been plasma ion nitrided, showing the nitrided layer on the left hand side.

Figure 2 depicts the hardness profile throughout the white layer and the diffusion zone. It starts at a surface hardness of 615 HV and approaches the hardness of the substrate at greater depths that is equal to 220 HV. Figure 2 also presents the surface profile of the percentage of Fe_4N nitride within the white layer, which is shown in the inset to superimpose on the hardness profile.

The x-ray residual stress measurements were performed from the surface until a depth of 1 mm, which corresponds to the mid surface of the fatigue sample, equivalent to the neuter line during the alternated fatigue stress cycling. This data is shown in figure 3, which also includes an inset that amplifies the first 200-μm-depth profile.

Figure 4 shows the Wöhler curves corresponding to the substrate and plasma ion nitrided steels with and without previous hydrogen charging. It is clear that the plasma ion nitriding substantially increases the fatigue resistance of the material, the fatigue limit changing from 360 MPa (curve 1) for the substrate to 660 MPa (curve 3) for the nitrided sample. As expected, the presence of hydrogen in the material promotes an important decrease of the fatigue limit.

The optical microscopy Nomarski interferometry was useful to verify the fatigue crack initiation and the fatigue damage accumulation for each of the samples tested. This is shown in figures 5 through 8 for two different percentages of the fatigue life for the as received steel (figure 5), the nitrided one (figure 6) and for these materials tested after hydrogen charging (figures 7 and 8).

Discussion

The hardness of the nitrided layer is equal to about 615 HV within the white layer, decreases rapidly to about 540 HV in the first 5 μm of the diffusion zone, before diminishing at a small rate throughout the rest of the diffusion zone, to approach the substrate hardness at about 550 μm of depth.

The white layer, its increased hardness (figure 2) and its compressive stress state (figure 3), containing essentially the γ'-Fe_4N nitride, depicted in figure 1 and profiled in figure 2, is the main responsible for the enhancement in the fatigue resistance of the steel tested. Figure 4 shows the Wöhler curves corresponding to the substrate and plasma ion nitrided steels with and without hydrogen. It is clear that the plasma ion nitriding substantially increases the fatigue resistance of the material, the fatigue limit changing from 360 MPa (curve 1) for the substrate to 660 MPa (curve 3) for the nitrided sample. It is remarkable though that the beginning of the plateau corresponding to the fatigue limit occurs much before, below 10^5 cycles, for the nitrided steel as compared to the as received material, when it appears after 10^6 cycles. This is probably due to the fact that the cyclic stress levels supported by the nitrided sample are so high that once crack initiation has occurred, the propagation kinetics is rather fast. The introduction of hydrogen by the previous hydrogen charging procedure resulted in a loss of mechanical properties in fatigue in

both types of samples. Although, the fatigue limit drop due to the presence of hydrogen was more marked for the nitrided steel, its value still remained well above that of the as received steel without hydrogen. This was so even taking into consideration that the nitrided steel was more strongly hydrogen charged than the as received steel, by considering that the nitrided layer acts as an important diffusion barrier for hydrogen, and that it is actually embrittled by hydrogen (6).

The surface damaging process due to the fatigue cycling differs for the as received steel and the nitrided one. For the former the fatigue damage follows very well the classical behavior observed for ductile materials. This includes increase in dislocation density, formation and growth of persistent slip bands, initiation and coalescence of surface micro-cracks to form a macro-crack responsible for the fatigue fracture of the specimen. Figure 5 (a and b) show the sequence of events demonstrated by optical microscopy with Nomarski interferometry associated with the cyclic loading of the as received samples. For the nitrided specimen neither persistent slip bands nor micro-crack initiation were observed at the sample surface, as shown in figure 6 (a and b). This is due to the white layer that impedes the formation of the surface persistent slip bands. The effect of hydrogen is apparent by the increase on the number of surface cracks as shown in figure 7 (a and b) for the as-received and hydrogenated steel, as well as in figure 8 (a and b) for the plasma ion nitrided and hydrogenated steel.

The initiation of the fatigue micro-crack, which grew to form the macro-crack responsible for the fatigue failure in the nitrided steel, with and without hydrogen, occurred subsuperficially. This became evident by the optical interferometric analysis, figures 6 b and 8 b, as well as by observing the fracture micromorphology using scanning electron microscopy. Such a behavior may be rationalized by considering the residual stress profile depicted in figure 3. One observes that there is a compressive stress state until a depth of about 550 μm and that the residual stress is locally important in the interface between the white layer and the diffusion zone. This becomes still more apparent if the resultant stress is determined, as a combination of the applied and residual stresses, such as shown in figure 9. In fact, the maximum value of the resultant stress is located in the vicinity of the white layer – diffusion zone interface region as it is well represented in figure 9. This local resultant stress maximum is the site of the fatigue subsurface micro-crack initiation.

Conclusions

1 The fatigue resistance of the API Type 5L X-65 steel is enhanced by plasma ion nitriding even when it has been previously charged with hydrogen. This behavior is accounted for by the presence of a nitrided layer bearing a compressive residual stress state, comprising a white layer of increased hardness that contains essentially the γ'-Fe_4N nitride;

2 The fatigue crack initiation in the as received steel follows the classical behavior observed for ductile materials, by presenting the formation of persistent slip bands and of surface micro-cracks that are created, grow and coalesce to form the main fatigue crack. The number of surface micro-cracks increase upon hydrogenation, leading to faster growth and coalescence;

3 The fatigue crack initiation in the nitrided steel occurs subsuperficially due to the existence of a peak on the resultant stress (combination of residual and applied stresses) at a site in the vicinity of the white layer – diffusion zone interface.

Acknowledgments

The authors acknowledge the financial support to this work by CNPq (grants nos. 523298/96-0; 467256/00-4); CAPES/COFECUB type II project no. 206/97-99 and FAPERJ grant no. E-26/151.944/2000.

References

1 Bathias C. (1999) There is no infinite fatigue life in metallic materials, Fatigue Fracture Engng. Mater. Struct. 22: 559-565.

2 Bott, A. H., Brühl, S. P., Gómez, B., Zampronio, M. A., Miranda, P. E. V. and Feugeas, J. N. (1998) Pulsed-plasma-nitrided API 5L X-65 steel: hydrogen permeability and microstructural aspects, Journal of Applied Physics. 31: 3469 – 3474.

3 Chen C. L., Lee P. Y., Chiou D. J., Chu C. Y., Lin J. Y., Wu J. K. (1993) Effect of nickel coating and inhibitors on hydrogen permeation steel. Journal of Materials Science Letters. 12: 205-206.

4 Chicot D., Bartier O., Zampronio M. A., Lesage J. and Miranda P. E. V. (1998) Diffusion et solubilité de l'hydrogène dans un acier faiblement allié nitruré ioniquement. La Revue de Métallurgie-CIT/ Science et Génie des Matériaux. 659-668.

5 Cruz, P. De la and Ericsson, T. (1998) Influence of seawater on the fatigue strength and notch sensitivity of a plasma nitrided B-Mn steel. Mat. Sci. And Engineering. A247: 204-213.

6. Lesage J., Chicot D., Bartier O., Zampronio M. A. and Miranda P. E. V. (2000) Influence of hydrogen contamination on tensile behavior of a plasma ion nitrided steel. Materials Science & Engineering A, 282: 203-212.

7 Sun Y. and Bell T. (1990) Plasma surface engineering of low alloy steel. Materials Science and Engineering. A140: 419-434.

8 Wang Q Y., Berard J. Y., Dubarre A., Baudry G., Rathery S. and Bathias C. (1999) Gigacycle fatigue of ferrous alloys. Fatigue Fract. Engng. Mater. Struct, 22: 667-672.

9. Zampronio M. A, Fassini F. D. and Miranda P. E. V. (1995) Design of ion-implanted contamination barrier layers for steel. Surf. & Coat. Tech.. 70: 203-209.

10. Zampronio M. A, Filevich A. and Miranda P. E. V. (1996) Hydrogen permeation behaviour of carbon ion implanted HSLA steel. Jounal of Materials Science Letters 15: 810-811.

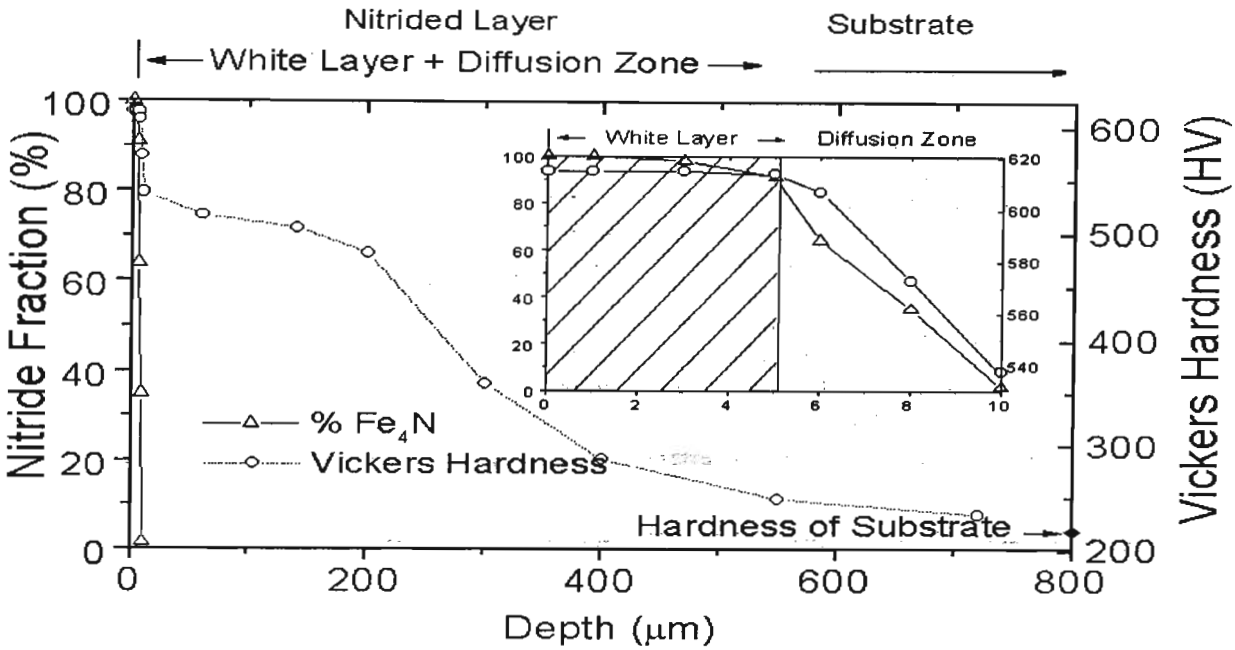

Fig. 2: Nitride fraction and hardness profile for the plasma ion nitrided steel

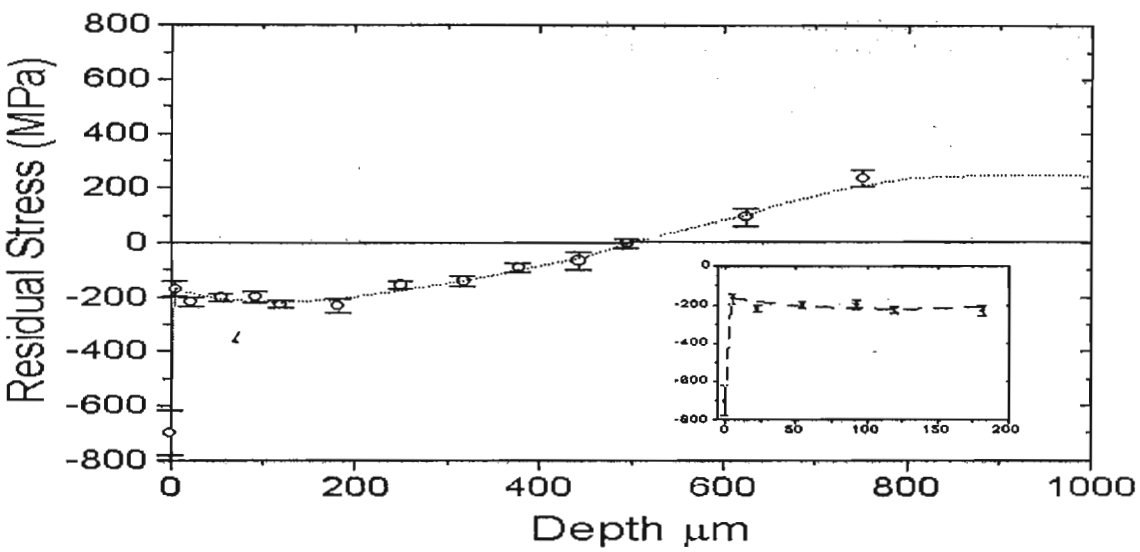

Fig. 3: Residual stress profile for the nitrided steel.

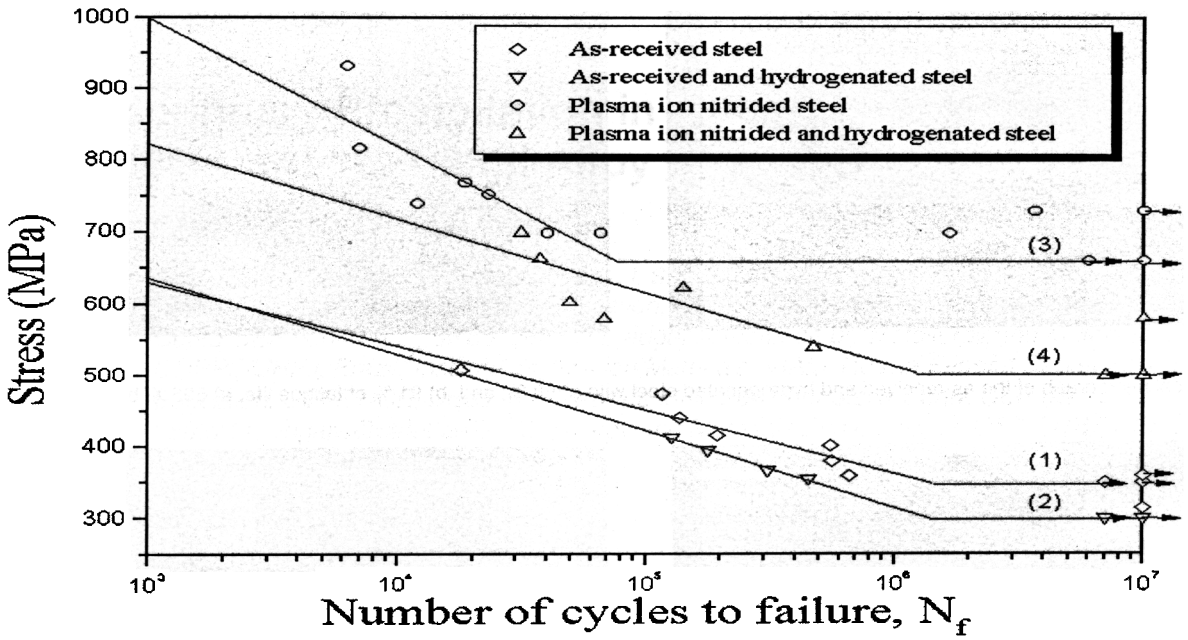

Fig. 4: Whöler curves for the as received and nitrided steels with and without hydrogen.

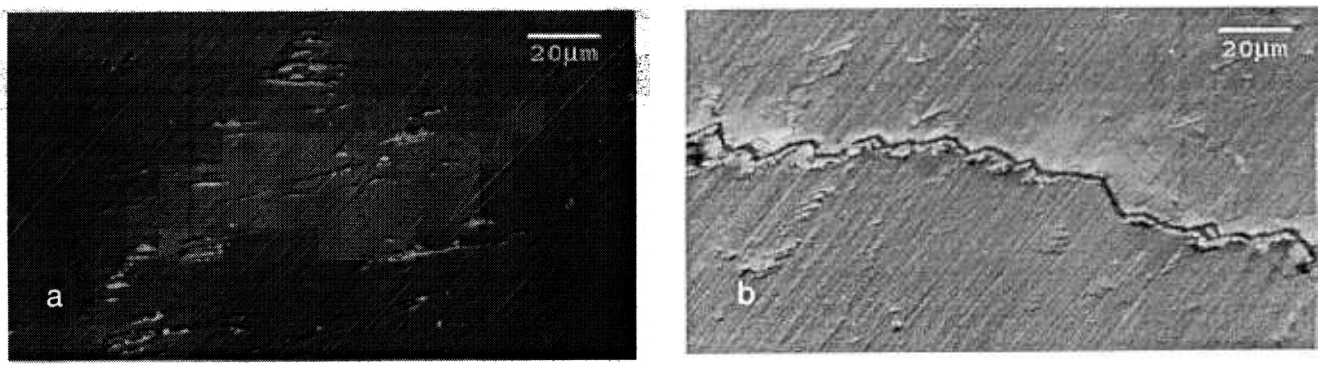

Fig. 5: Optical micrograph of the as received steel with a) 56 %; and b) 96 % of fatigue life. Original magnification: 595 X

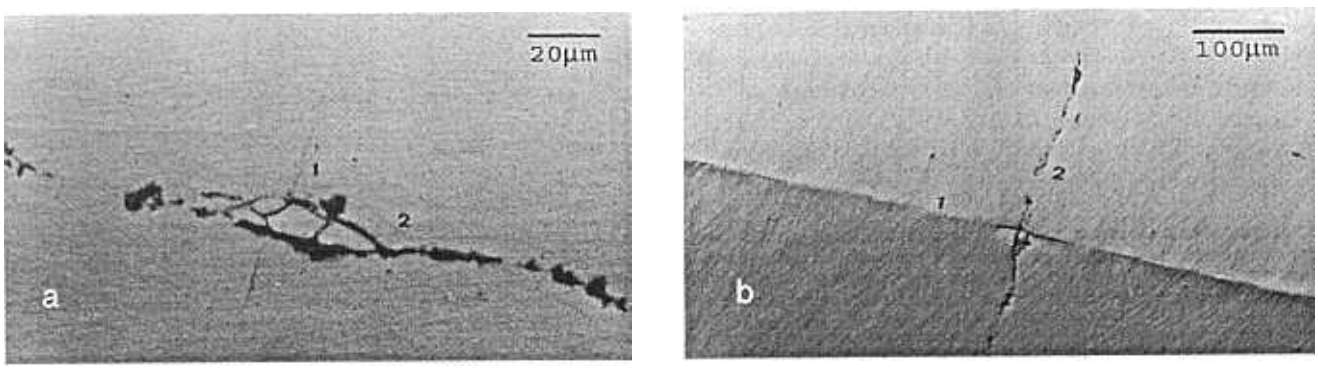

Fig. 6: Optical micrograph of the nitrided steel with a) 75 %; and b) 94 % of fatigue life. (1) surface micro-crack; (2) defect on the nitrided layer. Original magnification: a) 595 X; b) 151 X.

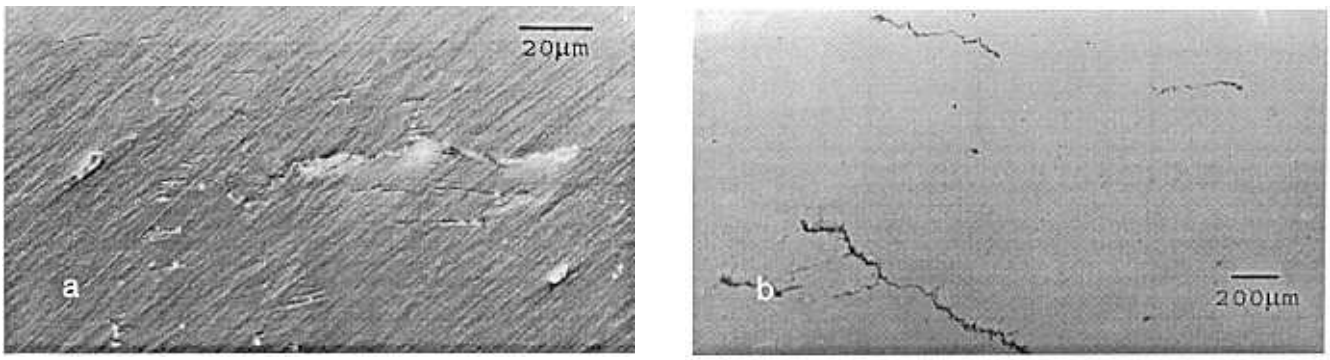

Fig 7: Optical micrograph of the as-received and hydrogenated steel with a) 68 %; and b) 91 % of fatigue life. a) 595 X; b) 38X

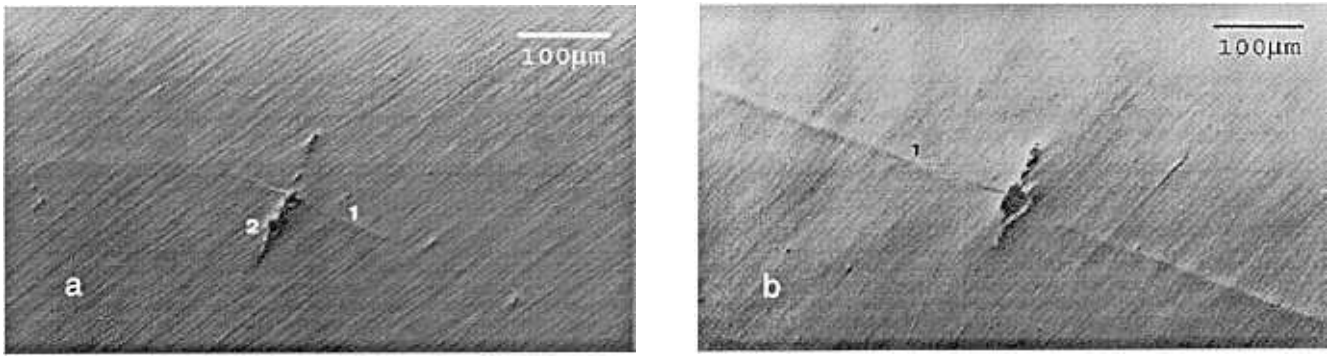

Fig. 8: Optical micrograph of the nitrided and hydrogenated steel with a) 75 %; and b) 82% of fatigue life. (1) surface micro-crack; (2) defect on the nitrided layer. Original magnification: 151 X.

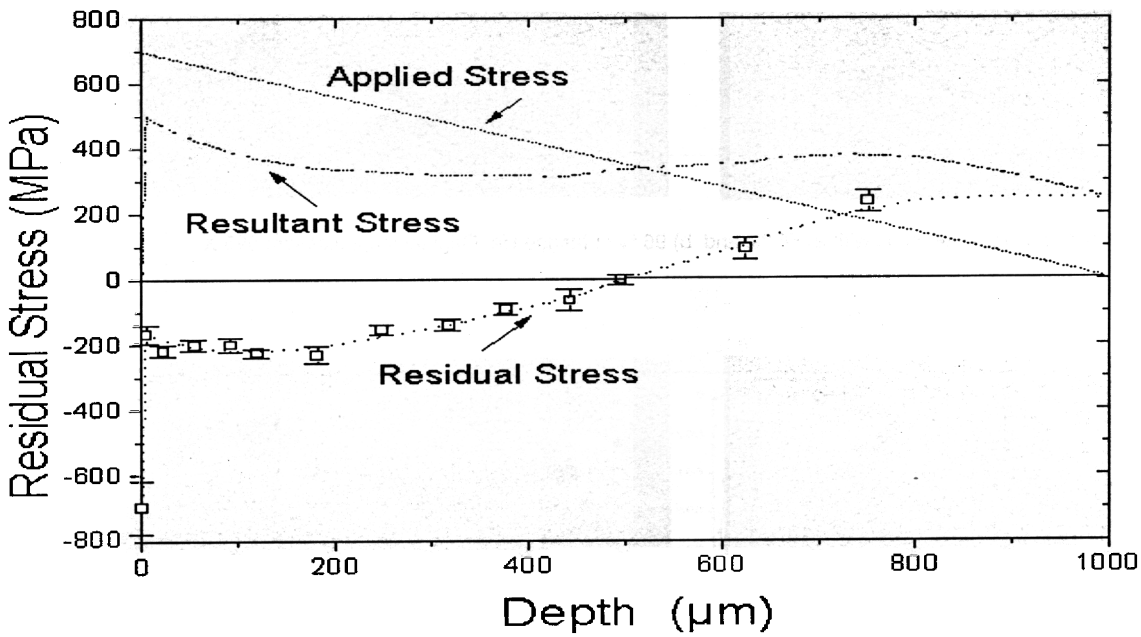

Fig9: Resultant stress as a combination of applied and residual stresses for the nitrided steel.